ELSEVIER

Catalysis Today 59 (2000) 151–162

CATALYSIS TODAY

www.elsevier.com/locate/cattod

# Mathematical modelling of catalytic combustors fuelled by gasified biomasses

G. Groppi [a,*], E. Tronconi [a], P. Forzatti [a], M. Berg [b]

[a] *Dipartimento di Chimica Industriale, Politecnico di Milano, Piazza Leonardo da Vinci 32, 20133 Milan, Italy*

[b] *TPS Termiska Processer AB, 611 82 Nyköping, Sweden*

**Abstract**

Catalytic combustion of low heating value (LHV) fuels from gasification of biomasses has attracted attention in recent years in order to reduce net $CO_2$ emissions in the atmosphere. A European project, ULECAT, has been undertaken to investigate this matter along with combustion of diesel fuel since 1996. This paper describes part of the work performed in the mathematical modelling task of this project in connection with the analysis of atmospheric pilot scale experiments.

Simulation results obtained with a single channel 2D model of the monolith catalyst are presented and compared with experimental results obtained in an atmospheric pilot scale facility. From this analysis a quantitative description of the role of the different governing phenomena in determining the combustor performance is derived and discussed to provide insight into the catalyst behaviour under severe conditions. The most critical parameters in the simulations are also identified and discussed. 

*Keywords:* Catalytic combustors; Gasified biomass; Pilot scale tests; Mathematical modelling; Monolith catalysts

## 1. Introduction

The use of low heating value (LHV) fuels from gasification of biomasses has attracted attention in recent years in order to reduce net $CO_2$ emissions in the atmosphere. Catalytic combustion may improve operation stability and decrease the formation of both thermal and fuel $NO_x$ in gas turbines fuelled with such LHV mixtures. A European project, ULECAT, has been undertaken to develop a dual fuel catalytic combustor suitable to burn gasified biomasses and diesel fuel since 1996. Project tasks include the specification of the characteristics of fuels and GT machines, the development of catalytic materials, pilot scale testing, mathematical modelling of the combustor and the analysis of the system on the basis of the results achieved in the different tasks. This paper describes part of the work performed in the modelling task in connection with analysis of the results of pilot scale experiments.

Mathematical models are recognized as important research tools in catalytic combustion for power applications. In particular, mathematical modelling, in addition to more conventional scale-up and design applications, can be regarded as a tool for fundamental investigation of the several and complex phenomena governing combustor performance.

Both distributed and lumped models are described in the literature and the subject has been recently reviewed [1,2]. Most of such models have been developed for the simulation of GT combustors fuelled by natural gas treated as a single component fuel (i.e.

* Corresponding author. Tel.: +39-2-23993258; fax: +39-2-70638173.
*E-mail address:* gianpiero.groppi@polimi.it (G. Groppi)

0920-5861/00/$ – see front matter 
PII: S0920-5861(00)00280-7

Table 1
Gas from gasification of wood and synthetic model gas mixture resembling the composition of the gasified biomass

| | CO (vol.%) | $CO_2$ (vol.%) | $H_2$ (vol.%) | $H_2O$ (vol.%) | $N_2$ (vol.%) | $CH_4$ (vol.%) | $C_2H_4$ (vol.%) | LHV ($MJ/m_n^3$) |
|---|---|---|---|---|---|---|---|---|
| Gasification gas | 15.4 | 11.8 | 12.6 | 10.0 | 47.1 | 2.6 | 0.4 | 4.5 |
| Synthetic model gas | 14.7 | 13.8 | 9.9 | 11.2 | 44.8 | 4.6 | 1.0 | 5.1 |

$CH_4$). Fuels from gasification of biomasses are quite complex mixtures mainly consisting of CO, $H_2$, $CH_4$ and, to a minor but significant extent, $C_2H_4$ as the major combustible components along with gasification byproducts, $CO_2$ and $H_2O$, and $N_2$ coming from gasification air. Besides minor amounts of tars, N- and S-containing compounds (mostly $NH_3$ and $H_2S$) are present which can markedly affect $NO_x$ formation and catalyst performance.

Under actual, pressurized (10–20 atm) conditions either transitional (laminar to turbulent) or turbulent regimes typically prevail in the channels of GT monolith combustors due to the extremely high specific flow rates. On the other hand, many pilot scale facilities, including the one developed in the ULECAT project, operate at atmospheric pressure. This typically corresponds to the laminar flow regime prevailing in the channels. In this latter case, and particularly in the presence of $H_2$-containing mixtures with high homogeneous reactivity and widely different diffusion rates of the fuel components, the use of distributed models is preferable to that of lumped ones, which may result in misleading predictions of heterogeneous and homogeneous ignitions and of gas–solid heat and mass transfer [2,3].

In this work analysis of the results obtained in the mathematical model of an atmospheric pilot combustor fuelled by gasified biomasses is presented. The simulation results of a 2D model of single channel of the monolith catalyst are presented in comparison with experimental data. The aim of the work is the quantitative description of the role of the different governing phenomena in determining the combustor performance in order to provide insight into the catalyst behaviour under severe conditions. The most critical parameters in the simulations are also identified and discussed.

## 2. Experimental

Pilot scale experiments have been performed in an atmospheric facility which is described in detail in a companion paper [4]. The experimental set up consists of a 30 kW, airblown, bubbling fluidized bed connected to a combustor rig with an inner diameter of 78 mm. The gasifier is fed with wood chips. The average composition of the fuel gas, after cleaning from particles in a cyclone and high temperature particulate filters, is reported in Table 1. The schematic of the combustor rig is shown in Fig. 1. The pilot operates under essentially adiabatic combustion conditions. The fuel gas is mixed with combustion air, which is electrically heated to enable the experiments to be performed with different inlet temperatures between 150 and 500°C. After mixing between the fuel gas and the combustion air, the mixture enters the combustion

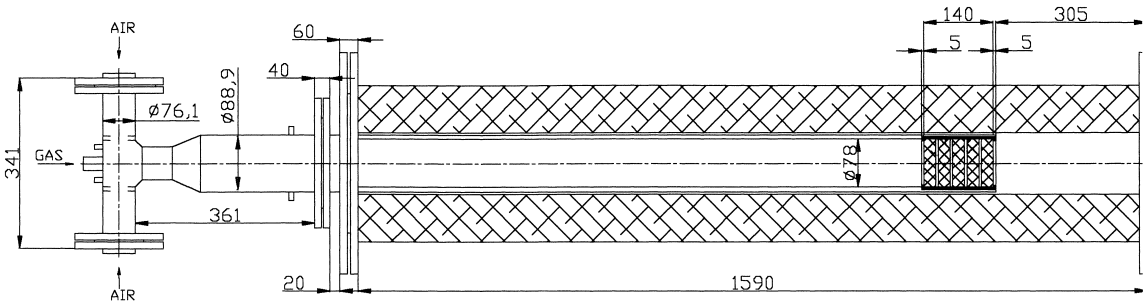


Fig. 1. Schematic of the pilot scale rig.

chamber and reaches the catalyst section. The diameter of the catalyst monoliths is 77 mm. One or several catalyst segments can be sequentially included. The total length of the combustion and mixing chamber from centre of the air pipe to the last catalyst is 1800 mm. The distance from the primary air flange to the outlet of the last catalyst can be varied but for all the experiments which are reported in this paper, the distance was 1600 mm in order to achieve a good mixing quality. Typically, deviations of the inlet concentrations from the mean value <1% have been measured.

Temperature measurements have been performed using one K-type thermocouple placed just upstream from the catalyst section and three thermocouples placed in the channels of the last catalyst segment at different axial and radial positions. In order to minimize the contribution of the homogeneous reaction downstream from the catalyst section, the sampling probe for the gas analysis was positioned 10 mm from the exit of the last catalyst segment. Analysis of CO and total hydrocarbons (THC) was performed by means of IR and FID, respectively.

Several catalyst configurations have been tested [4]. In this paper attention has been focused to two of them both consisting of one Pd-based catalyst segment followed by two Mn-substituted hexaaluminates (HA) segments. Both configurations adopted the same Pd-based catalyst, prepared by deposition on a cordierite monolith of a washcoat consisting of Pd supported on La-hexaaluminate. On the other hand, different HA segments have been used in the two configurations, namely extruded commercial HA catalysts and washcoated cordierite home made catalysts. Data on the characteristics of the different segments are reported in Table 2.

Due to the small scale of the gasifier, even minor fluctuations in the fuel feeding rate had a direct effect on both the amount and the quality of the fuel gas fed to the gasifier. The average heating value of this gas was 4.5 MJ/N m$^3$ but, due to the fluctuations in the fuel feeding rate, the heating value varied ±3% around this value. The flow rate of the fuel gas also had a variation of ±3% around the mean value with the higher flow rate corresponding to the higher heating value, thus both contributing to a higher fuel to air ratio and adiabatic temperature rise, since the combustion air was kept constant. This results in scattering of the experimental data. In particular strong simultaneous fluctuations have been observed for all the measured temperatures in the last catalyst segments that make difficult the analysis of *T*-profile data. However, preliminary analysis of the emission trends showed that scattering is markedly smoothened by plotting the experimental outlet concentrations of CO and THC versus the temperatures measured in the centre line of the last catalyst segments.

## 3. Model development

Based on the assumption of negligible heat dispersion and uniform distribution of variables at the inlet sections, a single channel description has been adopted for the monolith catalyst.

Ceramic honeycombs are typically extruded with square cells, but washcoat deposition results in corner rounding due to accumulation in the angles [5] and the actual geometry of the cross-section of a monolith cell is in between square and circular. In a preliminary study, a 2D description was found to provide similar

Table 2
Description of the simulated catalyst configurations (diameter 77 mm; length 2.3×3 cm)

| Segment No. | Catalyst type | CPSI | Void fraction | Washcoat thickness (μm) |
|---|---|---|---|---|
| *Configuration 1* | | | | |
| 1 | Washcoated Pd-catalyts | 200/12 | 0.589 | 62 |
| 2 | Commercial HA | 250/17 | 0.513 | Bulk |
| 3 | Commercial HA | 250/17 | 0.513 | Bulk |
| *Configuration 2* | | | | |
| 1 | Washcoated Pd-catalyts | 200/12 | 0.589 | 62 |
| 2 | Washcoated HA | 400/6.5 | 0.64 | 40 |
| 3 | Washcoated HA | 400/6.5 | 0.64 | 40 |

results to those obtained by a more complex 3D description. Accordingly, a 2D model has been adopted in this work. Model equations have been derived under the following assumptions along the lines described in a previous work [6]: (i) steady state conditions; (ii) fully developed laminar flow; (iii) negligible pressure along the monolith channel; (iv) negligible axial mass and heat diffusion in the gas phase; (v) negligible radiation effects, but for heat dispersion at the catalyst inlet; (vi) mass diffusion in the washcoat accounted for by analytical calculation of the effectiveness factor for the different catalytic reactions under the assumptions of first order reaction rate, slab geometry and isothermal washcoat thickness; (vii) *T*-dependent gas properties according to the following power laws:

$$D_i \propto T_g^{1.75}, \quad k_{tg} \propto T_g^{0.75}, \quad c_p \propto T_g^{0.2}$$

Kinetics for the heterogeneous reactions have been derived from laboratory tests on powder catalysts, assuming a first order dependence on fuel concentration. Homogenous reactions have been included using simple molecular kinetics from the literature [7,8]. Indeed the use of detailed schemes for the gas phase reaction of the C/H/O including ethylene would involve the description of 25–50 species depending on degree of reduction. Accordingly this would result in increasing the equation number by a 3–7 factor with a prohibitive increase of computational load using the solution algorithm described below. The presence of small amounts of tars, N- and S-containing compounds has been neglected.

The governing equations consist of one enthalpy balance and of *i*-species (CO, $H_2$, $CH_4$, $C_2H_4$, $CO_2$, $H_2O$ and $O_2$) mass balances for the solid and the gas phase and of a global mass balance for the gas phase.

The governing equations are given below with symbols explained in Section 6.

### 3.1. Governing equations

*Gas phase balances*:

$$\rho u \frac{\partial m_i}{\partial z} = \frac{1}{r}\frac{\partial}{\partial r}\left(\rho D_i r \frac{\partial m_i}{\partial r}\right) + M_i \sum_j v_{i,j} V_j^{\text{hom}} \quad (1)$$

$$\rho u c_p \frac{\partial T}{\partial z} = \frac{1}{r}\frac{\partial}{\partial r}\left(k_{tg} r \frac{\partial T}{\partial r}\right) - \sum_j \Delta H_{r,j} V_j^{\text{hom}} \quad (2)$$

*Solid phase balances*:

$$\frac{4\varepsilon}{d_{eq}} \rho D_i \left.\frac{\partial m_i}{\partial r}\right|_{r=R} = M_i \sum_j \xi v_{i,j} \eta_j V_j^{\text{het}} \quad (3)$$

$$(k_{ts}\lambda + k_{tw}\xi)\frac{\partial^2 T_w}{\partial z^2} + \frac{4\varepsilon}{d_{eq}} k_{t_g} \left.\frac{\partial T}{\partial r}\right|_{r=R} = -\sum_j \xi \Delta H_{r,j} \eta_j V_j^{\text{het}} \quad (4)$$

*Global mass balance*:

$$\int_A \rho u \, dA = \int_A \rho^0 u^0 \, dA \quad (5)$$

with

$$u = 2\bar{u}\left[1 - \left(\frac{r}{R}\right)^2\right] \quad (6)$$

*Boundary conditions*:
Inlet conditions ($z$=0)

$$T = T^0, \qquad m_i = m_i^0 \quad (7)$$

$$(k_{ts}\lambda + k_{tw}\xi)\frac{\partial T_w}{\partial z} = \sigma e (T_w^4 - T_{-\infty}^4) \quad (8)$$

Outlet condition ($z$=$L$)

$$\frac{\partial T_w}{\partial z} = 0 \quad (9)$$

Symmetry conditions at the channel axis ($r$=0)

$$\frac{\partial T}{\partial r} = \frac{\partial m_i}{\partial r} = 0 \quad (10)$$

Conditions at the catalytic walls ($r$=$R$):

$$T_w = T, \qquad m_{i,w} = m_i \quad (11)$$

Equations have been solved in dimensionless form. The numerical solution of the resulting PDE boundary value problem has been performed using orthogonal collocations for cross-sectional discretization and orthogonal collocation on finite elements [9,10] with adaptive grid mesh for axial discretization [11]. In the case of square cells, the geometrical symmetry has been taken into account so that only one eighth of the monolith channel cross-section has been considered as solution domain. The resulting set of AEs has been solved by means of a continuation method [12].

Typically, five radial collocation points and nine axial nodes are required to achieve numerical convergence, corresponding to 746 equations.

## 4. Simulation of the pilot scale rig

As mentioned above, despite some scatter, experimental data show well definite and complex trends that markedly depend on the adopted catalyst configuration [4]. Mathematical model simulations of the pilot scale rig have been performed aiming at the quantitative description of the role of the different governing phenomena in determining the combustor performance. Such an analysis is expected to provide insight into the catalyst behaviour under severe conditions.

In addition to data on fuel composition and characteristics of the catalyst configurations reported in Tables 1 and 2, the parameters related to operating conditions and to kinetics of heterogeneous and homogeneous reactions adopted in the simulations are reported in Tables 3 and 4. Simulations have been performed by fixing all conditions except for the inlet gas temperature which has been varied from 230 to 400°C.

Fig. 2a and b reports the calculated axial profiles of catalyst and cupmix gas temperatures. The use of catalyst segments with different activities results in different types of profiles. In the first segment consisting of a highly active Pd-based catalyst, a typical light-off behaviour is observed. On increasing the inlet temperature, steep axial gradients of the catalyst temperature appear, introducing an ignition front which progressively shifts towards the catalyst inlet. Upon ignition, the gas temperature progressively increases due to heat released by the catalyst wall, but due to short length of the catalyst segment and relatively high flow rates, it remains considerably below the catalyst temperature. According to the simulations, much smoother *T*-gradients occur in the segments consisting of HA-based catalyst, due to their low combustion activity. Indeed, when the temperature of the gas exiting from the first segment is too low, light-off does not occur at all. On the other hand, the rise of the gas temperature in the first segment up to the level required for ignition of the HA catalysts is associated with a depletion of the fuel content, and particularly of the more reactive CO–$H_2$ fraction, so that only a "weak" ignition of the HA catalysts is obtained also in this condition. As a result the calculated gas and catalyst temperatures in the HA-based monoliths are always close and, particularly in the last segment, where

Table 3
Simulation parameters for catalytic kinetics and operating conditions

| Catalytic kinetics $r_i = K_i C_i$ (mol/cm$^3$ s) | | |
|---|---|---|
| Species | $K^0$ ($s^{-1}$) at 653 K | $E_{act}$ (cal/mol) |
| *KTH Pd catalyst* | | |
| $H_2$ | 791 | 10500 |
| CO | 400 | 11000 |
| $CH_4$ | 20 | 21000 |
| $C_2H_4$ | 200 | 17000 |
| *HA catalyst* | | |
| $H_2$ | 13 | 13000 |
| CO | 75 | 15300 |
| $CH_4$ | 0.14 | 23900 |
| $C_2H_4$ | 0.28 | 19000 |
| *Operating conditions* | | |
| Pressure | 1 atm | |
| Flow rate (N m$^3$/h) | | |
| $W_{air}$ | 43.68 | |
| $W_{fuel}$ | 12.32 | |

Table 4
Homogeneous reaction kinetics[a]

| Species | Rate expression (mol/cm$^3$ s) | Pre-exponential factor | $E_{act}$ (cal/mol) |
|---|---|---|---|
| $H_2$ | $r = KC_{H_2}C_{O_2}$ [8] | $2.196\times10^{12}$ | 26100 |
| CO | $r = KC_{CO}C_{O_2}^{0.25}C_{H_2O}^{0.5}$ [7] | $3.98\times10^{14}$ | 40000 |
| $CH_4$ | $r = KC_{CH_4}^{0.7}C_{O_2}^{0.8}$ [7] | $1.58\times10^{13}$ | 48400 |
| $C_2H_4$ | $r = KC_{C_2H_4}^{0.7}C_{O_2}^{0.8}$ (this work) | $1.58\times10^{14}$ | 39700 |

[a] For combustion of hydrocarbon the following two-step global mechanism has been considered: (1) $C_nH_m + (0.5n + 0.25m)O_2 \rightarrow nCO + 0.5mH_2O$, (2) $CO + 0.5O_2 \rightarrow CO_2$.

experimental temperatures have been measured, they differ only by 10–20°C.

From calculated temperature profiles plotted in Fig. 2a, it is worth noting that when ignition occurs to a large extent in the first segment, the calculated temperature of the Pd-based catalysts markedly exceeds the theoretical value for PdO decomposition to Pd metal. At the experimental conditions investigated in this work (atmospheric pressure, $O_2$ molar fraction at the catalyst wall ranging from 0.13 to 0.15 depending on fuel consumption), a decomposition temperature of 1060–1070 K is obtained from thermodynamics [13]. It is widely reported in the literature [14–16] that in natural gas combustion, such a decomposition is associated with a marked drop of $CH_4$ combustion activity. To our knowledge no data have been reported on the relevance of this effect in the presence of important amounts of other fuel components; however, it can be conceived that the catalytic combustion of the $CH_4$ fraction is significantly inhibited upon PdO decomposition. In the absence of reliable correlations, one can roughly assume that $CH_4$ combustion activity of the Pd catalyst drops to zero once the light-off has occurred. The results obtained under such an assumption, which corresponds to set the $K^0_{CH_4}$ value in Table 1 equal to 0, are reported in Fig. 2b. Comparison with Fig. 2a shows that assuming the first catalyst inactive in $CH_4$ combustion results in a lower calculated temperature of the Pd-catalyst that, once ignition has completely occurred, remains well below the adiabatic reaction temperature due to the unreacted $CH_4$ fraction of the fuel. Nevertheless, it is still higher than the decomposition temperature of PdO, i.e. the combustion of the $H_2$–CO fraction of the fuel (and to a minor extent of $C_2H_4$) can be sufficient to rise the temperature of the catalyst above the PdO decomposition temperature. It is worth stressing that this behaviour would provide the basis for an effective control method of the temperature of Pd-based catalyst during combustion of mixtures from biomass gasification.

On the other hand only a minor effect of $CH_4$ combustion activity of the first segment on the ignition behaviour is observed. This is better illustrated in Fig. 3, where the $T_{out}$ versus $T_{in}$ plots, calculated assuming the Pd-based catalyst active or inactive in $CH_4$ combustion, are compared with the experimental curve. It is worth noting that the choice of the gas outlet temperature as the relevant parameter from the simulation

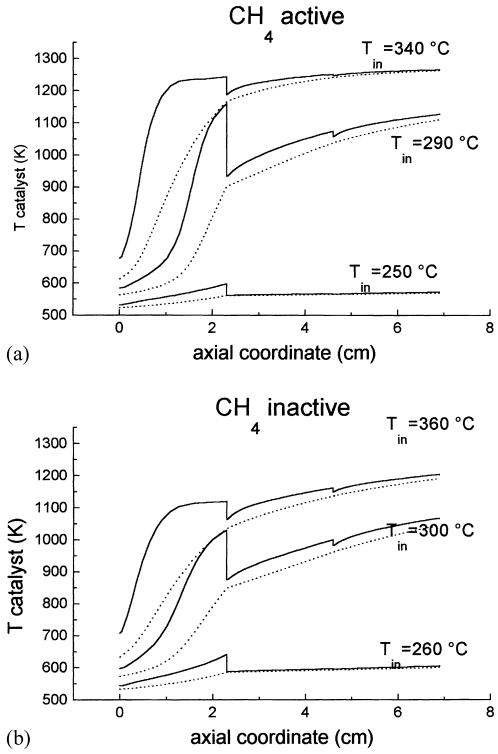


Fig. 2. Calculated axial profiles of catalyst and cupmix average gas temperatures. (a) First segment active in $CH_4$ combustion; (b) first segment inactive in $CH_4$ combustion.

for comparison with experimental results is not critical due to the mentioned similarity of calculated gas and catalyst temperatures in the last segment. Under both assumptions, an ignition temperature of about 270°C has been estimated. Indeed, ignition is governed by the

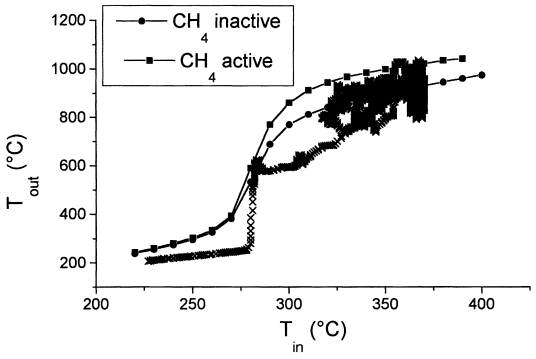


Fig. 3. Comparison of calculated with experimental ignition curves.

most reactive components (CO and $H_2$) [17], whose activities have been taken identical in both cases. The calculated value of light-off temperature compares well with the experimental one, although a steeper temperature increase is observed in the experiments.

At higher inlet temperature, significant differences are observed between the two calculated gas outlet temperatures. Once ignition has occurred, the assumption of negligible $CH_4$ activity of the first Pd-based segment results in a reduced $CH_4$ consumption, and consequently in a lower and more gradual outlet temperature rise. Noticeably also the experimental value apparently shows a similar progressive trend; however, the wide scatter of the data makes such a comparison difficult. It is worth noting that the assumption of negligible $CH_4$ combustion activity in the first segment has only a minor effect on the behaviour of the downstream HA catalysts that only exhibit a slightly steeper temperature increase along the axial coordinate, as shown in Fig. 2b. In fact, according to the simulations, the unreacted fuel from the first segment mostly consists of $CH_4$ that can hardly be ignited over HA catalysts at the temperature and residence time conditions of this work.

Despite reasonable agreement of temperature predictions, Fig. 4a and b shows that calculated emission trends are completely mismatched. By plotting the experimental outlet concentration of THC and CO as a function of the temperature measured in the last catalytic segment, the following typical trends are observed: THC, whose inlet concentration is about 7000 ppm, gradually decrease above 800°C and are completely consumed above 950°C; CO, whose inlet concentration is about 3%, shows a very smooth decrease from 7000 to 4500 ppm in the temperature range 800–930°C and only upon complete THC consumption, exhibits a marked decrease down to about 1000 ppm at 1000°C, thus introducing a characteristic "two slope" trend. On the other hand, calculated emissions show completely different trends. Calculated THC markedly depend on the $CH_4$ combustion activity assumed in the first segment. When activity is neglected, only a minor $CH_4$ consumption is predicted and emissions slightly decrease down to 3500 ppm at 980°C. When activity is considered, a larger $CH_4$ consumption is obtained, but decrease of THC outlet concentration with outlet temperature is still under-predicted. Complete THC consumption is

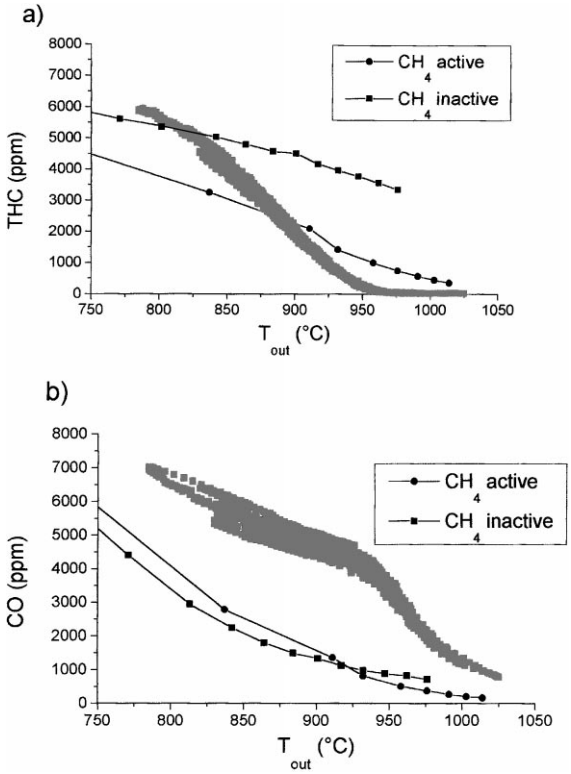


Fig. 4. Calculated versus experimental emissions. (a) THC emissions; (b) CO emissions.

approached only above 1000°C but never reached. Also calculated CO emissions show a markedly different trend from the experimental ones. Both on considering and neglecting $CH_4$ combustion activity in the first segment, the calculated outlet concentration of CO are well below the experimental ones and gradually decrease with outlet temperature reaching a plateau above 920–950°C.

Although some of the assumptions on the physical phenomena reported in Section 3 may not be rigorously satisfied, from the analysis of the governing equations it can be conceived that, at fixed catalyst geometry and operating conditions, calculated emissions mainly depend on the high temperature kinetics of heterogeneous and homogeneous combustion reactions. Both quantities are affected by large uncertainties. High temperature catalytic kinetics are obtained by extrapolation of laboratory data collected in the 100–400°C temperature range and are obviously extremely sensitive to activation energy estimates.

Besides different kinetic controlling mechanisms may prevail at widely different temperature ranges. On the other hand, it is well established that molecular kinetics give a very poor description of the complex reacting system in homogeneous combustion [18].

A sensitivity analysis of simulation results has confirmed the role of both catalytic and homogeneous high temperature kinetics. In particular the rate of reaction at the catalyst surface affects the combustor performance upon ignition, despite a strong influence of diffusional limitations. This is especially true in HA catalysts where, as evidenced by closeness of gas and catalyst temperature, a mixed chemical-diffusive regime prevails. Accordingly, on decreasing the activation energy of CO combustion over HA catalysts (i.e. on decreasing the high temperature reaction rate) a marked increase of calculated CO emission is obtained. However by simply adjusting the kinetic parameters of the catalytic reactions, it was not possible to fit the experimental emission trends. In particular the "two slope" behaviour of CO emissions was never obtained.

Hence, in order to better account for the experimental emission trends, the attention has been focused on homogeneous combustion rates. The literature expressions adopted in the simulation above were derived from experimental data obtained under conditions not far from those relevant to the present work but for the presence of other highly reactive fuel components such as $H_2$ and $C_2H_4$. It is well known that combustion of such components chemically activates oxidation of refractory $CH_4$ through generation of radical species able to extract a hydrogen atom resulting in the formation of a methyl radical [18]. To quantify this effect computational experiments have been performed using a detailed combustion reaction scheme [19] and simulating an isothermal plug flow reactor. Several effects have been investigated in the 800–1200°C temperature range including: reactivity of the single fuel components, two, three and four species interactions, influence of water, carbon dioxide and oxygen partial pressure. A comprehensive treatment of the results is in progress aiming at determination of generalized simple rate expressions to be used in the conditions relevant to catalytic combustion of gasified biomasses. Within the scope of this work only the major effect of $CH_4$ activation in the presence of $C_2H_4$ has been considered. Analysis of the results of computational

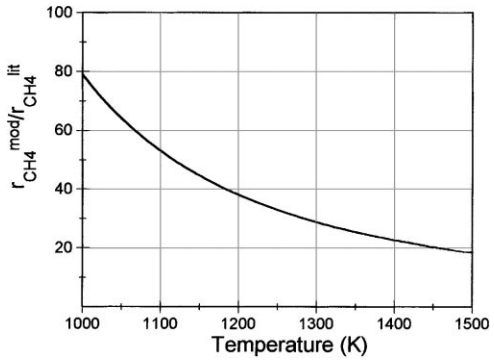


Fig. 5. $CH_4$ oxidation: ratio of modified to literature reaction rate.

experiments shows that this corresponds to a reduction of the apparent activation energy of $CH_4$ oxidation to 39 700 cal/mol also in the presence of limited $C_2H_4$ content. This value has been inserted in place of 48 700 cal/mol in the corresponding expression of Table 4 without changing any other parameter. Fig. 5 illustrates the resulting increase of $CH_4$ oxidation rate.

New simulations have been performed with the modified homogeneous kinetics under both the assumptions of the first catalyst segment active and inactive in $CH_4$ combustion. As expected, the light-off curves have not been substantially modified with respect to those reported in Fig. 3; indeed, ignition is governed by low-temperature catalytic activity and is not affected by homogeneous combustion rates. In Fig. 6a and b the emission trends of THC and CO calculated as a function of the gas outlet temperature are compared with the experimental results. It is evident that a much better match between model predictions and experiments has been achieved when assuming the first Pd-based segment inactive in $CH_4$ combustion. A progressive reduction of THC emissions is predicted above 800°C up to complete THC consumption at 950°C. Calculated CO emissions are lower than the experimental ones but exhibit the same qualitative trend with a smooth decrease up to the temperature at which THC combustion is completed (≅950°C) followed by a marked drop. As shown in Fig. 7a very good quantitative agreement can be obtained on decreasing the apparent activation energy of CO catalytic combustion over HA (i.e. by assuming a lower heterogeneous combustion rate at high temperature) by a quantity which is well within the experimental uncertainties. The enhancement of

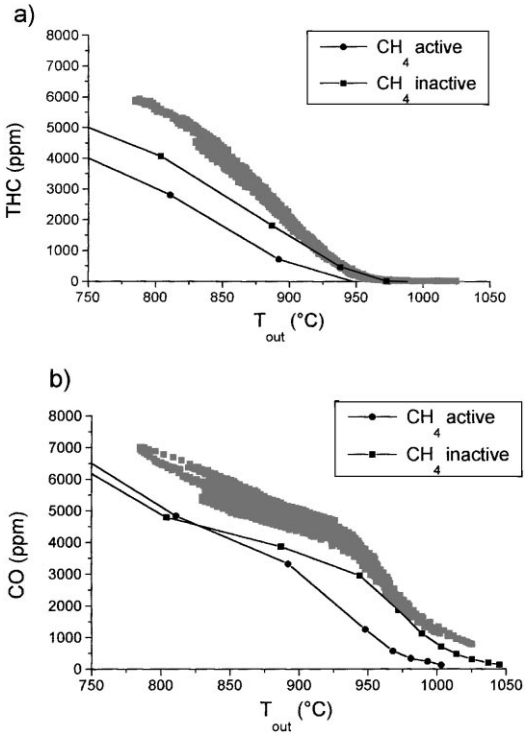


Fig. 6. Calculated versus experimental emissions with modified homogeneous kinetics. (a) THC emissions; (b) CO emissions.

homogeneous $CH_4$ combustion rate is responsible for modification of both THC and CO calculated emission trends. In fact $CH_4$ consumption via gas phase reaction is associated with formation of CO as intermediate oxidation product [19]. This can be clearly

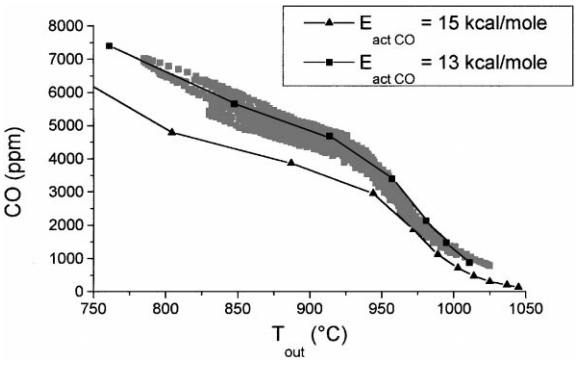


Fig. 7. Effect of activation of CO catalytic combustion over HA on calculated CO emission.

inferred from Fig. 8 where calculated conversion profiles of CO and $CH_4$ are compared with those associated with the contribution of the homogeneous reaction only. It is apparent that $CH_4$ mainly reacts in the gas phase, being scarcely consumed via catalytic reaction due to the assumption of zero $CH_4$ combustion activity for the Pd-based catalyst (first segment) and to the scarce activity in $CH_4$ combustion of hexaluminates (second and third segments). Besides, a negative contribution of the homogeneous reaction to CO consumption, related to the two step oxidation of $CH_4$, is evident. This additional production results in an enhancement of CO concentration with respect to that calculated considering only catalytic combustion, that under lean conditions oxidizes $CH_4$ directly to $CO_2$ over both noble metal [20] and HA [21,22] catalysts, and originates the observed "two slope trend". This effect was not appreciable using the literature kinetics derived from [7], the calculated rate of homogeneous $CH_4$ combustion being too slow to compete with catalytic combustion. Similarly this effect is not obtained when assuming that the first Pd-based catalyst is highly active in $CH_4$ combustion. Depletion of $CH_4$ in the first segment, where gas temperature is too low for homogeneous ignition, would markedly decrease the contribution of the gas phase reaction in the following HA catalysts. Accordingly, as shown in Fig. 6a and b, the calculated values of THC and CO emissions are much lower than the experimental ones. Although further verifications are needed this confirms that drop of $CH_4$ combustion activity due to PdO decomposition can be used as an effective control method of catalyst temperature in combustion of gasified biomasses.

In order to test the predicting capability of the model, the experiments using the synthetic fuel with composition reported in Table 1 have been simulated. Fig. 9a and b compares the experimental data and the calculated emissions obtained with fuel from the gasifier and with synthetic fuel, respectively. The experimental trends (Fig. 9a) clearly show that higher THC emissions are obtained with the synthetic fuel. Besides, in the same experiment CO emissions show a characteristic maximum associated with the marked drop of THC oulet concentration. Model simulations qualitatively predict such higher emissions of CO and THC that, according to model analysis, are both related to the higher $CH_4$ content of the synthetic fuel

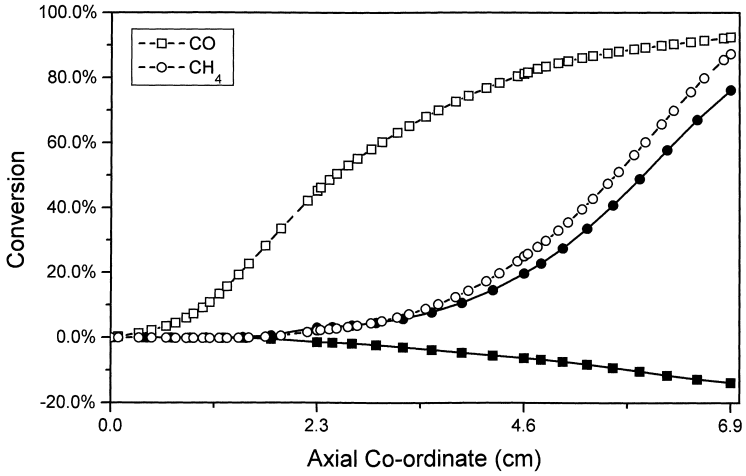


Fig. 8. Comparison of total (open symbols) and homogeneous combustion (solid symbols) conversion profiles calculated for $CH_4$ and CO.

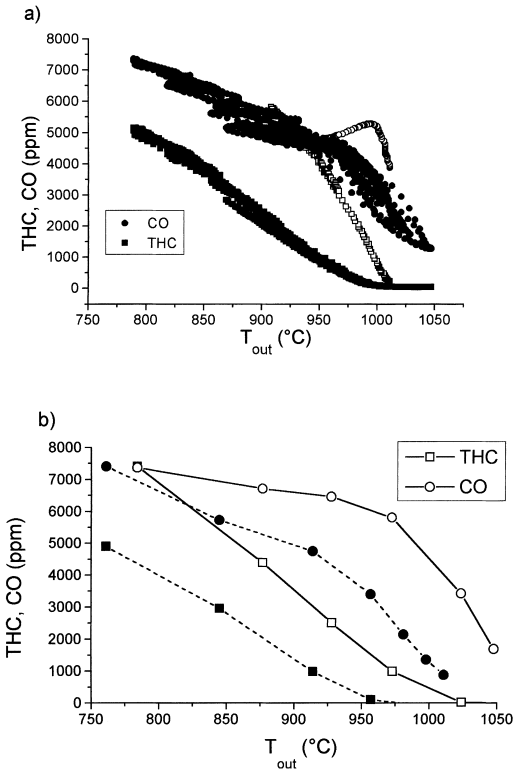


Fig. 9. Comparison of emission trends with synthetic (open symbols) and gasifier fuels (solid symbols). (a) Experimental results; (b) model predictions.

(see Table 1). From the quantitative point of view, the agreement of calculated and experimental values is not excellent. Indeed the model predicts a more gradual decrease of THC concentration and, consequently, does not predict the maximum in CO emissions. Such a lack of accuracy is likely to be related to the poor description of the gas phase combustion. Further refinements of the homogeneous rate expressions were beyond the scope of this work. However, in the case of the experiments with synthetic fuel, model predictions provide quantitative evidence in favour of high-T homogeneous combustion of $CH_4$ and drop of catalytic activity in $CH_4$ combustion over the first Pd-based catalyst being the phenomena responsible for the observed emission trends.

Also the other catalyst configuration described in the experimental section, consisting of the same Pd-based segment followed by two washcoated HA/cordierite (400/6.5 cpsi) monoliths prepared at KTH University, has been simulated. Calculated emissions are reported in Fig. 10 in comparison with those obtained in the simulations for the configuration with commercial HA catalysts. Similar emission trends have been obtained for the two catalyst configurations. This is in line with the experimental results that provide the same qualitative emission trends for the two configurations [4] and confirms the reliability of model predictions.

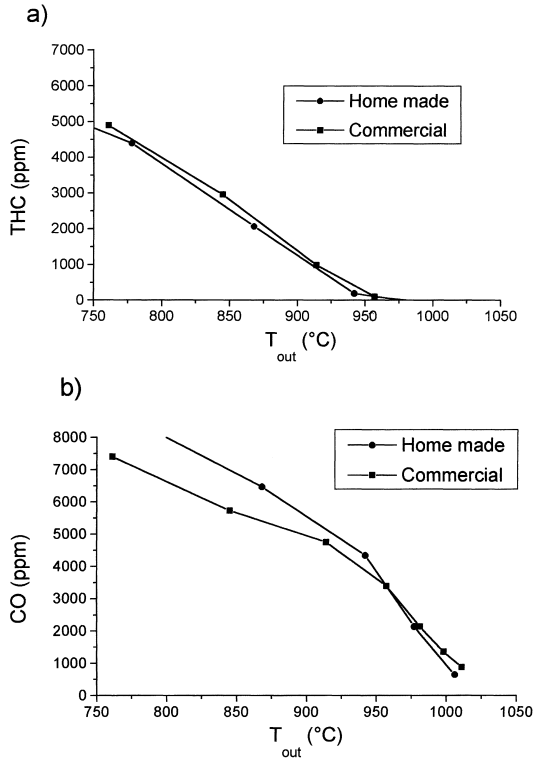


Fig. 10. Comparison of catalyst configuration with commercial and home made HA catalysts in the last two segments. (a) THC emissions; (b) CO emissions.

## 5. Conclusions

Mathematical modelling of an atmospheric pilot catalytic combustor of gasified biomasses has been demonstrated as a powerful tool for the analysis of complex trends of experimental temperature and emission data. Model analysis has allowed to discriminate the role of catalytic and homogeneous reactions and related kinetics in determining light-off and emission performances. In particular simulation results have provided indications that drop of $CH_4$ combustion activity due to PdO decomposition also occurs in the presence of complex reacting mixtures and that this can be used as an effective control method of catalyst temperature in combustion of gasified biomasses.

To achieve such goals, the model must provide an accurate description of both physical and chemical phenomena, a task which is particularly demanding for combustion of multicomponent fuels.

In the analysis of calculated emission trends a critical role of both high temperature catalytic combustion kinetics and of homogeneous combustion rates has emerged. Both these parameters suffer from large uncertainties in the conditions relevant to catalytic combustion for power applications. In this work the problem has been addressed by "tuning" the rate expressions on the basis of both chemically consistent assumptions (e.g. homogeneous activation of $CH_4$ by $C_2H_4$ and $H_2$) and feedback from fitting to experimental results. However, further efforts are required from both the experimental and the theoretical side in order to develop fully predictive models.

## 6. Nomenclature

| | |
|---|---|
| $A$ | channel cross-section ($m^2$) |
| $c_p$ | mass specific heat (J/kg K) |
| $D_i$ | mass diffusivity of $i$-species ($m^2$/s) |
| $d_{eq}$ | equivalent diameter of the monolith channel (m) |
| $\Delta H_{r,j}$ | heat of $j$-reaction (J/mol) |
| $e$ | emissivity factor |
| $h$ | heat transfer coefficient (W/$m^2$ K) |
| $K_m$ | mass transfer coefficients (kg/$m^2$ s K) |
| $k_t$ | thermal conductivity (W/m K) |
| $m_i$ | mass fraction of $i$-species |
| $M_i$ | molar weight of $i$-species (kg/kmol) |
| $L$ | catalyst length (m) |
| $r$ | radial coordinate (m) |
| $R=d_{eq}/2$ | channel radius (m) |
| $T$ | temperature (K) |
| $u$ | gas velocity (m/s) |
| $V_j$ | rate of $j$-reaction (mol/$cm^3$ s) |
| $z$ | axial coordinate (m) |

*Greek letters*

| | |
|---|---|
| $\alpha$ | thermal diffusivity ($m^2$/s) |
| $\varepsilon$ | void fraction |
| $\phi_j$ | Thiele modulus of catalytic $j$-reaction |
| $\eta_j=\mathrm{Th}(\phi_j)/\phi_j$ | efficiency factor of catalytic $j$-reaction |
| $\lambda$ | inert support fraction |
| $\nu_{i,j}$ | stoichiometric coefficients of $i$-species in $j$-reaction |

| | |
|---|---|
| $\rho$ | density (kg/m$^3$) |
| $\sigma$ | Stefan–Boltzmann constant ($5.67\times10^{-8}$ W/m$^2$ K$^4$) |
| $\xi$ | active washcoat fraction |

*Superscripts and subscripts*

| | |
|---|---|
| g | gas phase |
| het | heterogeneous reaction |
| hom | homogeneous reaction |
| 0 | inlet conditions |
| s | inert support |
| w | active washcoat |

## Acknowledgements

This work has been performed under UE contract JOR3-CT96-0071. The authors wish to thank Prof. Tiziano Faravelli of Politecnico di Milano for his assistance on homogeneous combustion rates.

## References

[1] R.E. Hayes, S.T. Kolaczkowski, Introduction to Catalytic Combustion, Gordon and Breach, London, 1997.
[2] G. Groppi, E. Tronconi, P. Forzatti, Catal. Rev. Sci. Eng. 41 (2) (1999) 227.
[3] G. Groppi, A. Belloli, E. Tronconi, P. Forzatti, Chem. Eng. Sci. 50 (1995) 2705.
[4] M. Berg, E.M. Johansson, S.G. Jaras, Catal. Today 59 (2000) 117.
[5] D. Leung, R.E. Hayes, S.T. Kolaczkowski, Can. J. Chem. Eng. 74 (1996) 94.
[6] G. Groppi, A. Belloli, E. Tronconi, P. Forzatti, AIChE J. 41 (1995) 2250.
[7] F.L. Dryier, I. Glassmann, in: Proceedings of the 14th International Symposium on Combustion, Vol. 987, The Combustion Institute, Pittsburgh, PA, 1972.
[8] T. Mitani, F.A. Williams, Combust. Flame 39 (1980) 169.
[9] B. Finlayson, Nonlinear Analysis in Chemical Engineering, McGraw-Hill, New York, 1980.
[10] L.C. Young, B.A. Finlayson, AIChE J. 22 (1976) 331.
[11] G. Groppi, E. Tronconi, Chem. Eng. Sci. 55 (2000) 2161.
[12] T.C. Wayburn, J.D. Seader, Comp. Chem. Eng. 11 (1987) 7.
[13] H. Kleykamp, Z. Physik. Chem. N.F. 71 (1970) 142.
[14] R.J. Farrauto, M.C. Hobson, T. Kennelly, E.M. Waterman, Appl. Catal. A 81 (1992) 227.
[15] R.A. Dalla Betta, N. Ezawa, K. Tsurumi, J.C. Schlatter, S.G. Nickolas, US Patent 5 183 401, 2 February 1993.
[16] P. Forzatti, G. Groppi, Catal. Today (and references therein), 54 (1999) 165.
[17] G. Groppi, L. Lietti E. Tronconi, P. Forzatti, Catal. Today 45 (1998) 159.
[18] I. Glassmann, Combustion, 3rd Edition, Academic Press, New York, 1994.
[19] E. Ranzi, A. Sogaro P. Gaffuri, G. Pennati, T. Faravelli, Combust. Sci. Technol. 95 (1994) 1.
[20] R.A. Dalla Betta, D.G. Loffler, Heterogeneous hydrocarbon oxidation, ACS Symp. Ser. 638 (1996) 36.
[21] M. Machida, K. Eguchi, H. Arai, J. Catal. 103 (1987) 385.
[22] G. Groppi, M. Bellotto, C. Cristiani, P. Forzatti, P.L. Villa, Appl. Catal. A 104 (1993) 101.